CERN-ACC-NOTE-2018-0005
29-01-2018
ivan.karpov@cern.ch

HOM power in FCC-ee cavities

Ivan Karpov, Rama Calaga, Elena Shaposhnikova (BE-RF)
CERN, Geneva, Switzerland

Keywords: FCC-ee, HOMs, power losses, beam spectrum, impedance calculation

Summary

This Note summarizes the results of the power loss calculations for FCC-ee machines with 400.79 MHz cavity options. The requirements for the single-cell cavity design and for the operation with beam are obtained from the results for the high-current FCC-ee machine (Z). For other machines the power loss is sufficiently low and can be absorbed and extracted by foreseen HOM couplers.

1 Introduction

The heat load produced by a beam passing through the accelerator structures can cause significant limitations for the machine performance. To determine parameters for high order mode (HOM) absorbers accurate estimations of the power loss are required, which depend both on the beam parameters and the design of RF cavities. Here, we present calculations for several options of beam and machine parameters of the FCC-ee collider [1] which are summarized in Table 1. We also discuss the results for an earlier set of parameters of the Z machine [2], where the bunch spacing of 2.5 ns was fixed due to a large number of bunches. For the latest parameters the number of bunches is almost 4 times smaller which means that different values of the bunch spacing can be used in operation and need to be analyzed.

For calculations of the power loss from a circulating beam, the following equation is used

$$P = J_A^2 \sum_{k=-\infty}^{+\infty} \mathrm{Re}\left[Z_\parallel(k\omega_0)\right] \left|\hat{J}_k\right|^2 , \tag{1}$$

where J_A is the average beam current, $Z_\parallel$ is the longitudinal impedance, $\hat{J}_k$ is the normalized Fourier harmonic of the beam current at the k-th revolution harmonic, $\omega_0 = 2\pi f_0$, and f_0 is the revolution frequency. The analytical expressions of Fourier harmonics for different filling patterns and a Gaussian bunch line density are presented in Sec. 2. The longitudinal impedance spectrum and the loss factor of cavities obtained from simulations are described in Sec. 3. In Sec. 4 we present the results of power loss calculations. The work is concluded in Sec. 5.

Table 1: FCC-ee baseline parameters used for power loss calculations in this work [1]. An earlier set of parameters of the Z machine [2] are noted as Z (Berlin). The bunch length is given for the cases of colliding beams including beamstrahlung (BS) and non-colliding beams (no BS).

Parameter	Units	Z (Berlin)	Z	W	H	$\mathrm{t\bar{t}}$
Circumference, C	km	97.75				
Harmonic number, h		130680				
RF frequency, f_{RF}	MHz	400.79				
Beam energy, E	GeV	45.6		80	120	175
Beam current, J_A	mA	1400	1390	147	29	6.4
Number of bunches per beam, M		71200	16640	2000	393	48
Bunch population, N_{p}	10^{11}	0.4	1.7	1.5	1.5	2.7
Total bunch length (BS), σ	ps	12	40	25.5	16.3	10.8
Total bunch length (no BS), σ	ps	7	12	11	10.5	8.2
Momentum compaction factor, α_p	10^{-6}	14.79		7.31	7.31	7.31
Synchrotron tune, Q_s		0.041	0.025	0.023	0.036	0.069
Longitudinal damping time, τ_{SR}	turns	1281		235	70	23
Total RF voltage, V_{tot}	GV	0.255	0.1	0.44	2	9.5

2 Beam spectrum calculation

We consider a beam containing M bunches which can be grouped in n_{tr} equal trains with a distance between heads of the trains t_{tt}. This distance should be a multiple of bunch spacings t_{bb}. Each train contains a number of filled buckets $M_{\mathrm{b}} \leq t_{\mathrm{tt}}/t_{\mathrm{bb}}$. The beam has a regular filling which can also contain an abort gap of length t_{gap}. Arbitrary filling schemes would require additional tedious analysis with many degrees of freedom and therefore are not considered in the present work.

The time structure of the beam current $J(t)$ can be written, similarly to Ref. [3]

$$J(t) = \sum_{n=0}^{n_{\mathrm{tr}}-1} \sum_{m=0}^{M_{\mathrm{b}}-1} j(t - nt_{\mathrm{tt}} - mt_{\mathrm{bb}}) = J_A \sum_{k=-\infty}^{\infty} \hat{J}_k e^{-2\pi k f_0 t} \,, \tag{2}$$

where $J_A = n_{\mathrm{tr}} M_{\mathrm{b}} N_{\mathrm{p}} e f_0$ is the average beam current, and $j(t)$ is the single bunch current. For a Gaussian bunch with the rms bunch length σ (in seconds),

$$j(t) = \frac{eN_{\mathrm{p}}}{\sqrt{2\pi}\sigma} \exp\left\{-\frac{t^2}{2\sigma^2}\right\} \,. \tag{3}$$

The normalized Fourier harmonic of the beam current is

$$\hat{J}_k = \frac{\sin\left(n_{\mathrm{tr}}\pi k f_0 t_{\mathrm{tt}}\right)}{n_{\mathrm{tr}}\sin\left(\pi k f_0 t_{\mathrm{tt}}\right)} e^{i(n_{\mathrm{tr}}-1)\pi k f_0 t_{\mathrm{tt}}} \times \frac{\sin\left(M_{\mathrm{b}}\pi k f_0 t_{\mathrm{bb}}\right)}{M_{\mathrm{b}}\sin\left(\pi k f_0 t_{\mathrm{bb}}\right)} e^{i(M_{\mathrm{b}}-1)\pi k f_0 t_{\mathrm{bb}}} \times e^{-2(\pi k f_0 \sigma)^2} \,. \tag{4}$$

The number of bunches and trains which will fit in the machine depends on the abort gap length which is assumed to be $t_{\mathrm{gap}} = 2$ μs for this study. There are two sets of lines with the largest amplitude in the beam spectrum:

– at the multiple of frequencies $1/t_{\rm tt}$ (the first part of Eq. (4)) given by the train spacing,
– at the multiple of frequencies $1/t_{\rm bb}$ (the second part of Eq. (4)) given by the bunch spacing.

Depending on the filling scheme one can define two different regimes. The spectrum of the beam containing the large number of trains ($n_{\rm tr} \gg M_{\rm b}$) is dominated by lines with the distance $1/t_{\rm tt}$ (the left-hand side plot in Fig. 1). For the case of long trains ($n_{\rm tr} \leq M_{\rm b}$), the spectrum mainly contains lines at harmonics of $1/t_{\rm bb}$ corresponding to the bunch spacing and the maximum amplitude reduction of spectral lines between them is $1/M_{\rm b}^2$ (the right-hand side plot in Fig. 1).

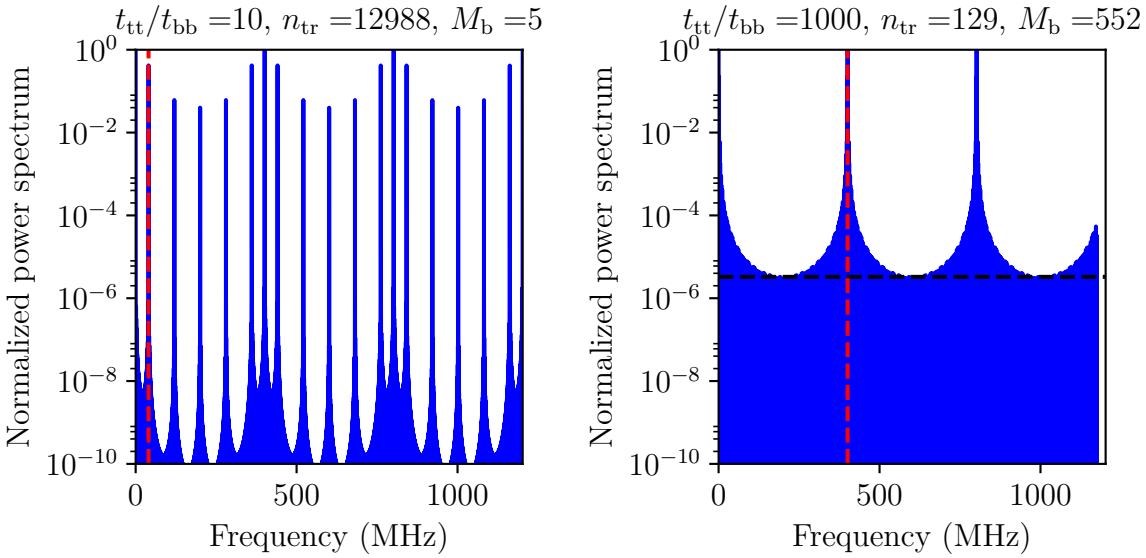

Fig. 1: Examples of the normalized beam spectra (the earlier set of parameters of the Z machine with $t_{\rm gap} = 2$ μs) for two regimes. The left-hand side plot is for the case of the large number of trains. The red line is at $1/t_{\rm tt}$. The right-hand side plot is the case of long trains. The red line is at $1/t_{\rm bb}$, and the horizontal black line is $1/M_{\rm b}^2$.

3 Impedance calculation

The 400 MHz LHC-like cavities [4] with different number of cells (single-cell, two-cell, and four-cell cavities) were considered in the present study of the FCC-ee rings (Fig. 2). Four cavities of these types with two tapers at the ends are placed in a single cryomodule (Fig. 3). The taper-out corresponds to the transition from the smaller radius b to a larger radius d and the

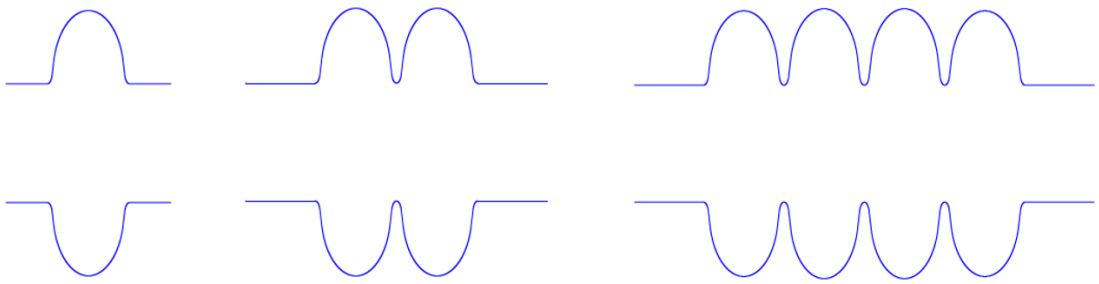

Fig. 2: LHC-like cavity designs with different number of cells (single-cell, two-cell, and four-cell cavities).

taper-in vice versa. The ABCI code [5] was used for impedance calculations of axi-symmetric perfectly conducting structures.

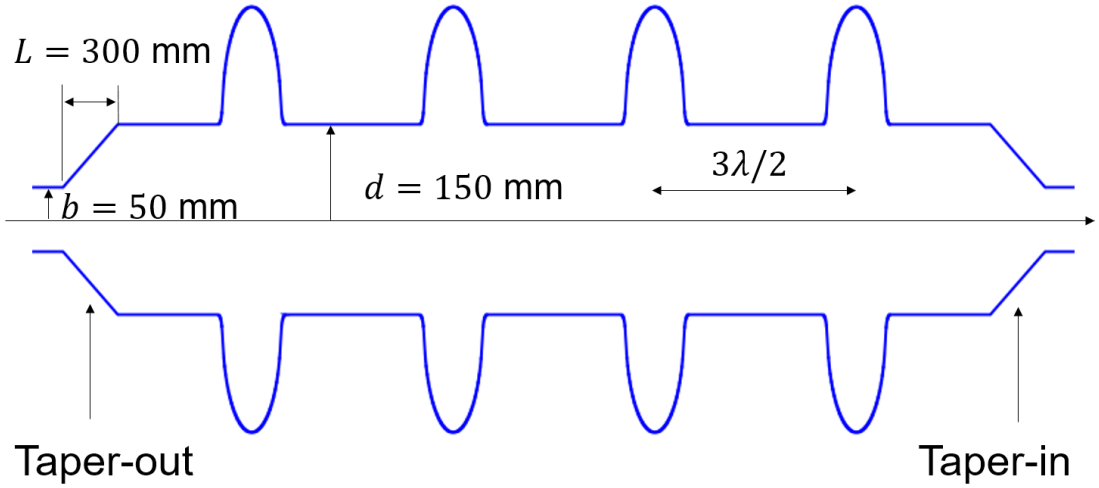

Fig. 3: Example of the LHC-like cryomodule containing four single-cell cavities and tapers.

3.1 Cavity impedance

The impedance of cavities with different number of cells and the fundamental frequency of 400.79 MHz was calculated for two frequency ranges: below 3 GHz, which contains "discrete" spectrum, and above 3 GHz, which contains "continuous" spectrum (Fig. 4). We can assume that the cutoff frequencies of all trapped HOMs are below 3 GHz for the beam pipe radius of 150 mm. In superconducting cavities the fundamental mode has a large quality factor $Q \sim 10^9$. It means that it is necessary to calculate a very long wake potential to get an accurate impedance value of this mode. In most cases, it is computationally expensive and a truncation of the wake potential should be used. This results in a smaller impedance of the fundamental mode and artificial impedance oscillations around it (see Fig. 4). Thus, the accurate impedance value of the fundamental mode and HOMs below the cutoff frequency can not be obtained, while the resonant frequency and the ratio of the shunt impedance and the quality factor R/Q of these modes can be extracted. The simulation parameters for both frequency ranges are summarized in Table 2. To resolve resonances at low frequencies simulations with long bunches and long wakes were used. For higher frequencies it is sufficient to use short wake potentials. It was found that artificial impedance peaks appear at high frequencies for a coarse mesh. Keeping the mesh size of 0.1 mm allows this problem to be avoided for frequencies below 40 GHz.

Table 2: Parameters used in ABCI simulations with results shown in Fig. 4.

Parameter	$f < 3$ GHz	$f > 3$ GHz
Bunch length [cm]	3.6	0.1
Wake potential length [m]	50	1
Radial mesh size [mm]	0.5	0.1
Longitudinal mesh size [mm]	0.5	0.1

Comparing the impedances of different cavity designs, we see that for a larger number of cells per cavity, the impedance is larger and more inevitable passband modes are present.

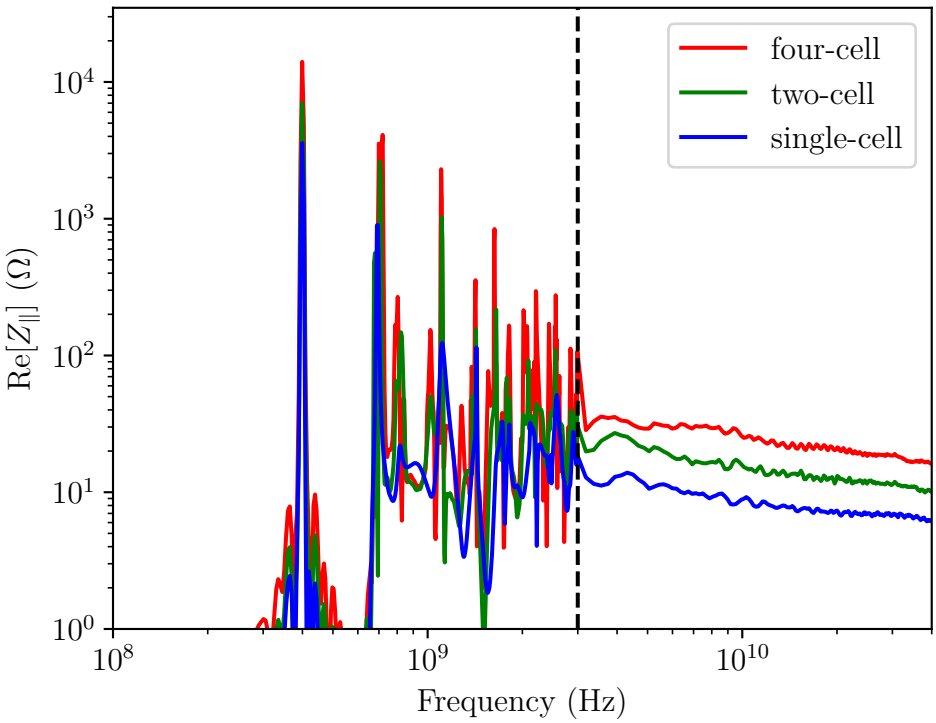

Fig. 4: The real part of longitudinal impedance of cavities with different number of cells obtained by using the ABCI code. The vertical dashed line is at 3 GHz. Additional impedance oscillations around fundamental mode are due to wake potential truncation (see Table 2).

It means that four-cell cavity design might not be feasible for the Z machine due to a high probability of hitting a resonance line by one of the beam spectral lines.

To verify the results obtained with ABCI code, we construct the loss factor $\kappa_{\parallel}$ as a function of frequency from the results of CST EM STUDIO® (CST EMS) [6] simulations

$$\kappa_{\parallel}(f) = \sum_n k_n \, \Theta[f - f_n] e^{-(2\pi f_n \sigma)^2} \,, \tag{5}$$

where Θ is the Heaviside step function and the modal loss factor of the n-th mode is

$$k_n = \pi f_n \left(\frac{R}{Q}\right)_n \,. \tag{6}$$

Here, f_n is the frequency of the n-th resonance mode, $(R/Q)_n$ is the ratio of the shunt impedance and the quality factor of this mode. There is a very good agreement between the two codes for frequencies below the cutoff frequency of the TM_{010} mode $f_{\mathrm{cut}} = 2.405c/(2\pi d) = 765$ MHz for the pipe radius $d = 15$ cm (Fig. 5). For higher frequencies the difference is due to the fact that CST EMS solver does not support open boundary conditions at the ends of the beam pipe. In this case, there are additional steps in the loss factor due to trapped modes in a pill-box cavity with smaller radius. According to simulations for all cavities, only a few resonant modes are present below cutoff frequency. The parameters of these modes are summarized in Table 3.

3.2 Taper impedance and loss factor

Tapers are used to make a smooth transition from the large beam pipe radius d inside the cryomodule to the smaller beam pipe radius b outside it. For a fixed ratio d/b, the contribution of tapers to the total impedance of the structure depends on taper length L. The worst situation is a

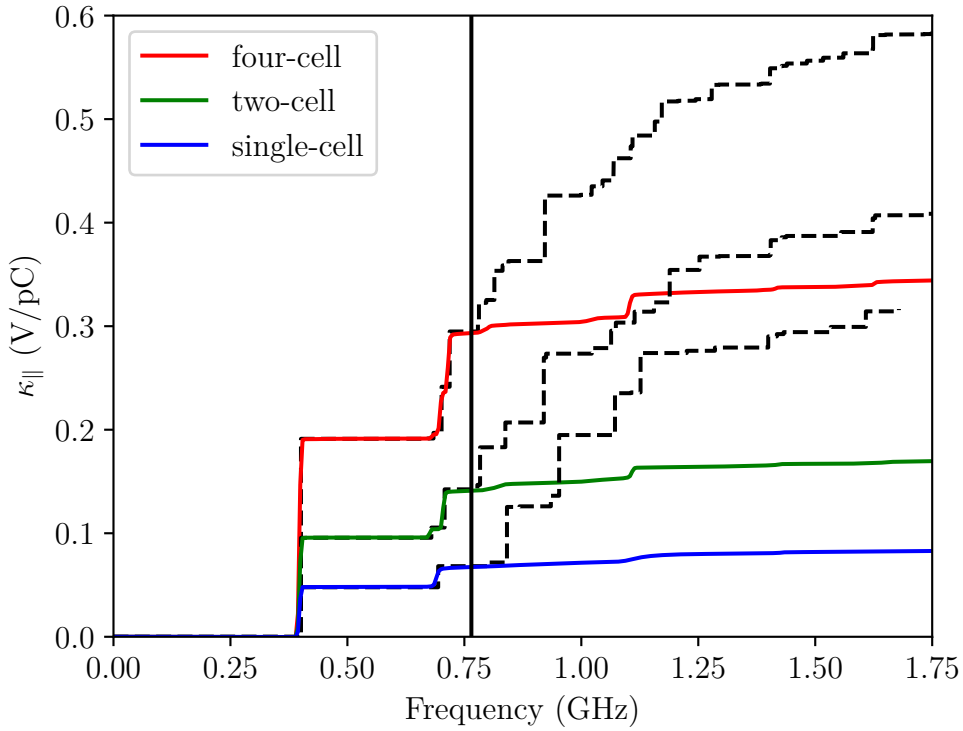

Fig. 5: The loss factor as a function of frequency obtained from ABCI for different number of cells. The dashed lines are the calculated loss factors from CST EMS results using Eq. (5). The solid vertical line is the cutoff frequency for the beam pipe radius of 15 cm ($f_{\mathrm{cut}} = 765$ MHz).

Table 3: Parameters of the fundamental mode and HOMs with highest R/Q below the cutoff frequency (CST EMS simulation results). The circuit definition is used for R/Q values.

Mode	f_{r} [MHz]	R/Q [Ω]
single-cell cavity		
Fundamental	400.98	42.3
HOM 1	694.03	11.7
two-cell cavity		
Fundamental	400.73	84.4
HOM 1	679.52	4.9
HOM 2	707.94	22.5
four-cell cavity		
Fundamental	400.72	168.5
HOM 1	671.27	0.2
HOM 2	684.06	2.6
HOM 3	701.38	24.7
HOM 4	718.66	34.8

step transition ($L = 0$), which can result in a significant increase of the longitudinal impedance at frequencies $f \gg c/2\pi d$. The impedance of the step-in and step-out can be calculated analytically in all frequency ranges [7]. For frequencies above cutoff a simple expression can be

used [8]

$$Z_{\rm step} = \frac{Z_0}{\pi} \ln\left(\frac{d}{b}\right) \ , \tag{7}$$

where $Z_0 = 120\pi\ \Omega$ is the impedance of free space.

Simulated impedance spectra (ABCI) of the taper-out for $b = 5$ cm, $d = 15$ cm, and different taper length are shown in Fig. 6. At low frequencies the impedance starts from non-zero value $Z_{\rm step}/2$ and then saturates to the value $Z_{\rm step}$ at higher frequencies. For a step-out ($L = 0$) the spectrum contains resonant peaks at lower frequencies, which disappear for longer tapers. For large L impedance remains constant at low frequencies (for $L = 3$ m, f below 10 GHz) and reaches the saturated value at high frequencies.

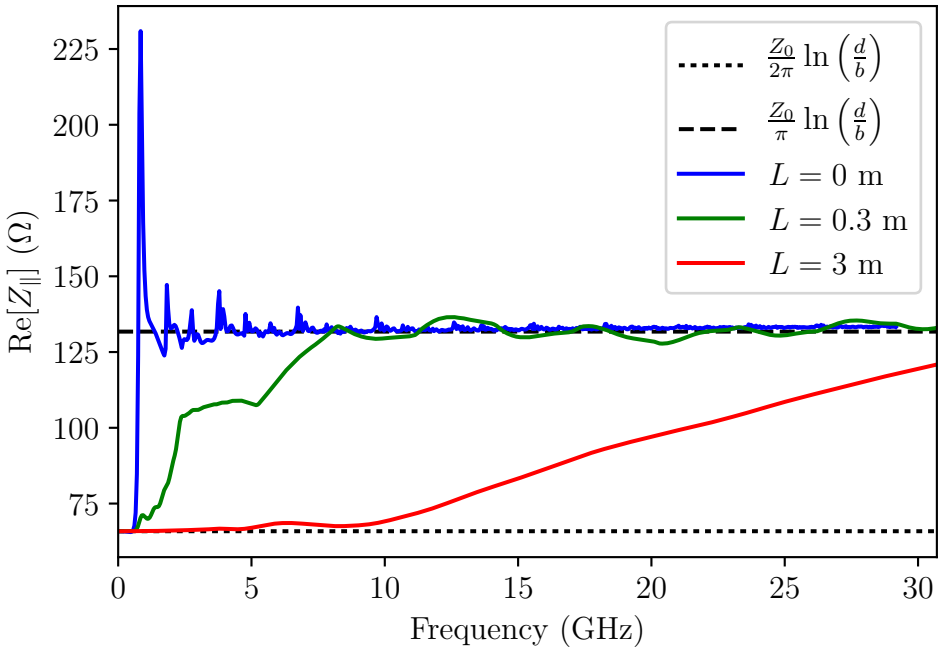

Fig. 6: The impedance spectrum for different lengths of the taper-out (ABCI simulation results).

The loss factor of a taper-out $\kappa_{\rm taper}$ as a function of taper length can be approximated as [8],

$$\kappa_{\rm taper} = \kappa_{\rm step} \times \left\{1 - \frac{1}{2}\min\left[1, \frac{L}{\tilde{L}}\right]\right\} \ , \tag{8}$$

where the loss factor of a step is

$$\kappa_{\rm step} = \frac{Z_{\rm step}}{2\sigma\sqrt{\pi}} \ , \tag{9}$$

and

$$\tilde{L} = \frac{(d-b)^2}{c\sigma} \tag{10}$$

is the "optimum" length, which corresponds to the minimum value of the taper loss factor. For a bunch length of 12 ps, $\tilde{L} \approx 2.7$ m. A smaller value of the loss factor for a longer taper is a result of the lower value of the impedance within the bunch spectrum. Fig. 7 shows consistency of the loss factors obtained by ABCI for different taper lengths with analytic predictions.

To calculate the loss factor of two tapers one has to assume some structure between them. For the simplest case, when a beam pipe of radius d and length $L_{\rm str}$ is tapered from both sides

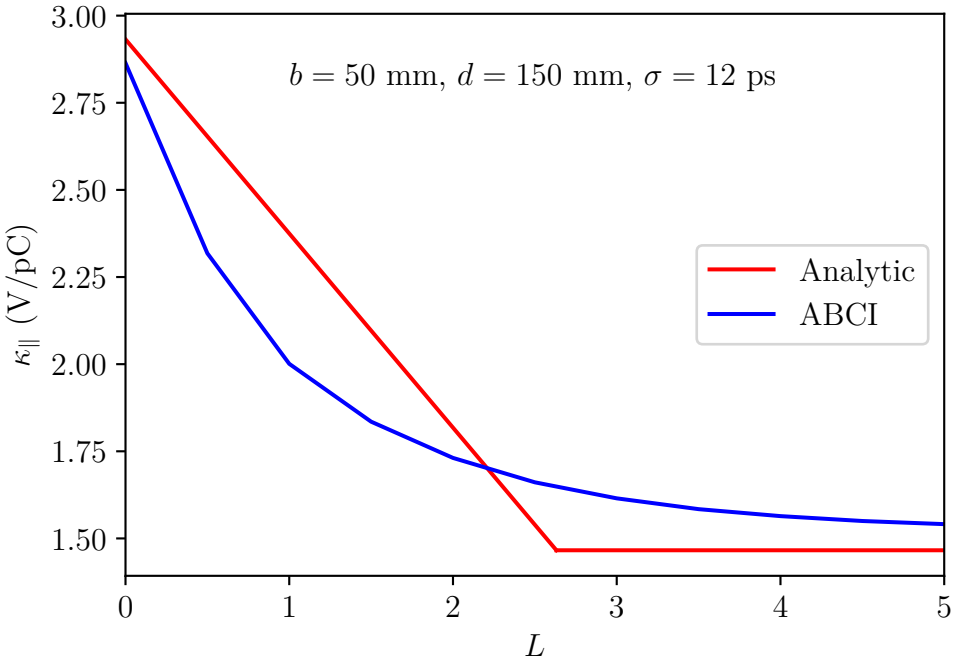

Fig. 7: Comparison of the loss factor of a taper-out from simulations (ABCI) and analytic predictions using Eq. (8) for different taper lengths.

to radius b using the tapers with length L, the analytic expression can be obtained [9]. If $L_{\rm str}$ fulfills the condition

$$L_{\rm str} \gg \frac{d^2}{c\sigma} \,, \tag{11}$$

the loss factor of two tapers is

$$\kappa_{\rm tapers} = \frac{Z_{\rm step}}{2\sigma\sqrt{\pi}} \left[\frac{2}{\pi} \arctan\left(\frac{0.2d^2}{c\sigma L}\right)\right]^2 \,. \tag{12}$$

For $L \gg d^2/c\sigma$ there is a significant reduction of $\kappa_{\rm tapers}$. This can be understood from the fact that impedances of the taper-in and taper-out are the same but the latter is shifted by $Z_{\rm step}$ value (Fig. 8). If we sum these impedances we see that the total impedance (the blue line) has a small value for the frequencies containing the bunch spectrum (the black line).

3.3 Simulations of full structure

Considering the case of the full structure which includes cavities and tapers, we need to clarify if there is a cancellation of the impedance contributions from the taper-in and the taper-out. For results of simulations shown below we assume that four single-cell cavities are separated by a distance of 2λ ($\lambda = 0.748$ m for $f_{\rm RF} = 400.79$ MHz) and combined in a single cryomodule. The tapers ($L = 3$ m) are placed at a distance λ from the center of the last cavities (Fig. 9).

Comparison of the low frequency impedances (below 3 GHz) of the full structure with step and taper transitions is shown in Fig. 10. There are more resonant lines in the spectrum for the case of step transition than for the case of long tapers. This is due to an additional long cavity produced by two steps. The results obtained by ABCI code are also confirmed by CST EMS results by comparing the loss factor as a function of frequency (see, Fig. 11). If we compare the impedance spectra of only four cavities and four cavities with tapers one can see that they are almost identical (Fig. 12). However, there is a difference from the single-cell impedance, which

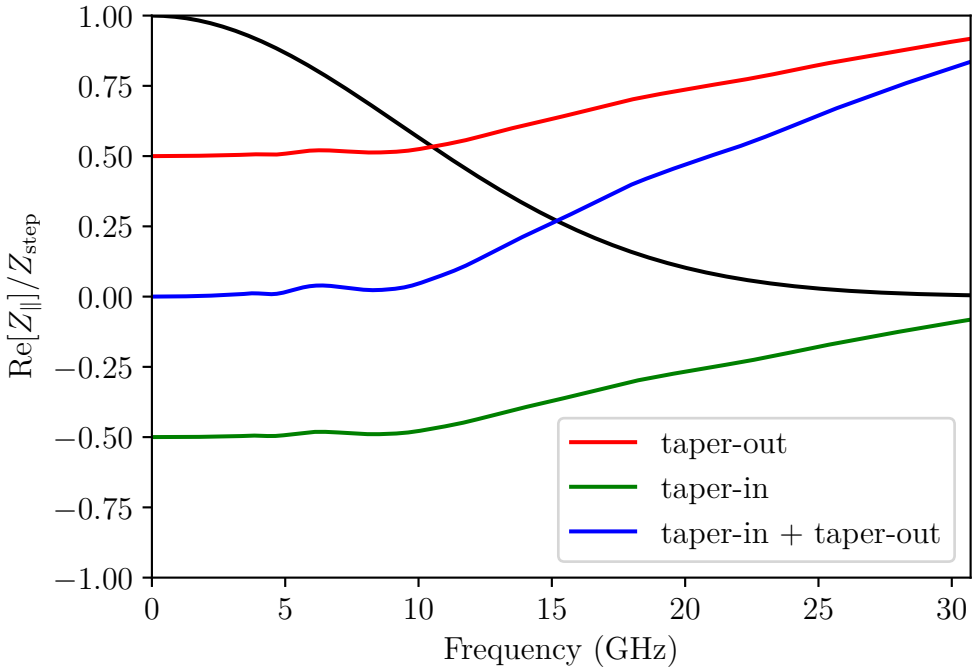

Fig. 8: The normalized impedance spectra of taper-in and taper-out from simulations for $b = 50$ mm, $d = 150$ mm, and $L = 3$ m. The black line is the envelope of the normalized single-bunch power spectrum for $\sigma = 12$ ps.

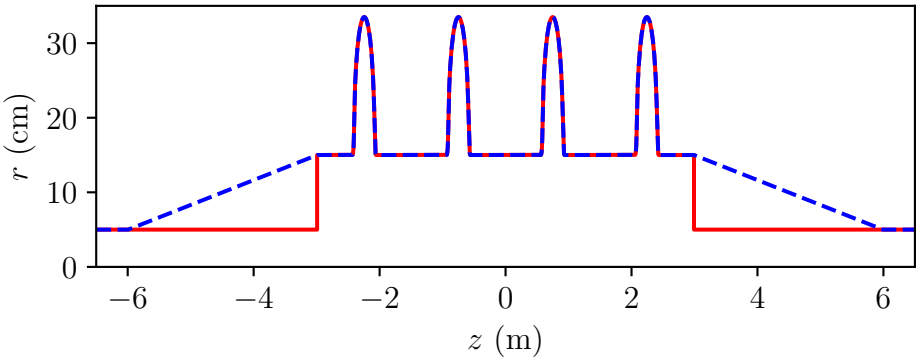

Fig. 9: The full structure of four single-cell cavities with tapers used in simulations.

contains fewer resonance lines. This could be due to the coupling of the HOMs of cavities in the cryomodule, which is not present for a single cavity.

The calculations of the contribution of different components to the total loss factor of the structure are summarized in Table 4. Without cavities, there are some discrepancies between simulation results and analytic estimations for steps, taper-out, and tapered cavity using Eq. (9), Eq. (8), and Eq. (12), correspondingly. This could be due to the resonant modes excited in the long cavity which contribute to the total loss factor. For the case of two tapers the difference is also because a distance between tapers ($L_{\mathrm{str}} \approx 6$ m) does not fulfill the condition given by Eq. (11) for a bunch length of 12 ps ($d^2/c\sigma = 5.9$ m).

To evaluate the results of the full structure the loss factor of four single-cell cavities was also calculated for the beam pipe without tapering ($\kappa_{4\mathrm{cav}} = 1.22$ V/pC). For the step transitions the total loss factor is dominated by the contribution of the steps, but is not given as the sum of $\kappa_{4\mathrm{cav}}$ and κ_{step}. The loss factors of the structures with taper-out and two tapers are significantly

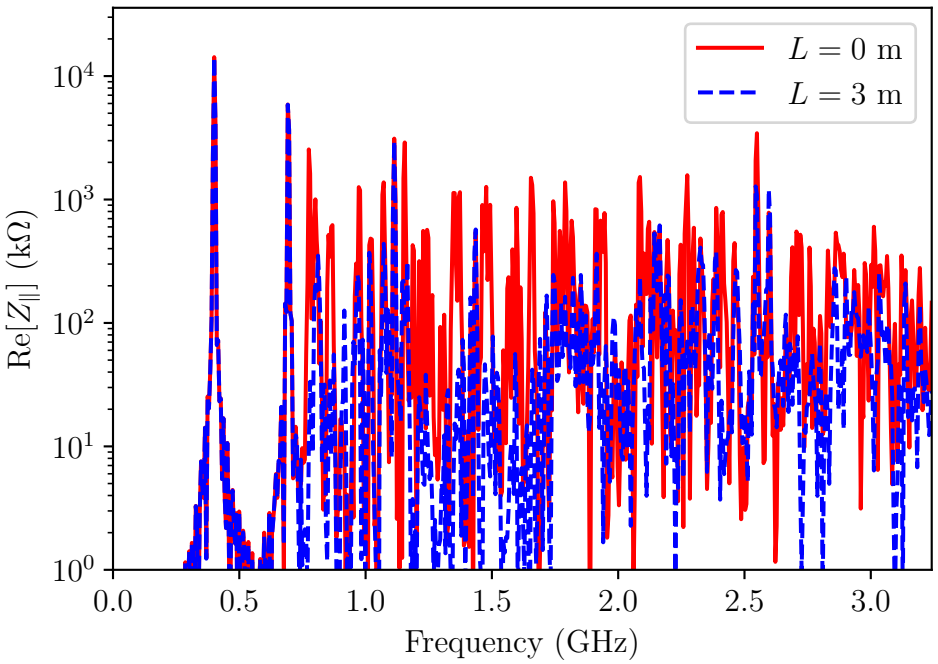

Fig. 10: Impedances of the full structure of four single-cell cavities with step ($L = 0$) and taper transitions (see Fig. 9).

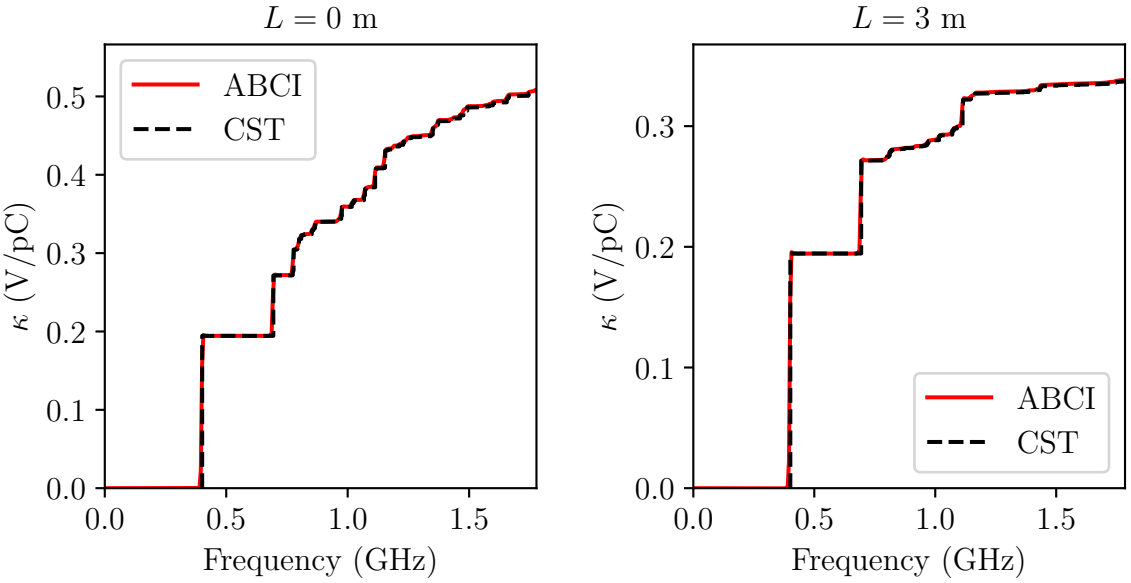

Fig. 11: The loss factor as a function of frequency obtained from ABCI for the full structure of four single-cell cavities combined with steps (the left-hand side plot) and tapers (the right-hand side plot). The dashed lines are the calculated loss factors from CST EMS results using Eq. (5).

smaller in comparison to the case of step transitions. However, contributions of two tapers are not anymore fully compensated as in the case without cavities.

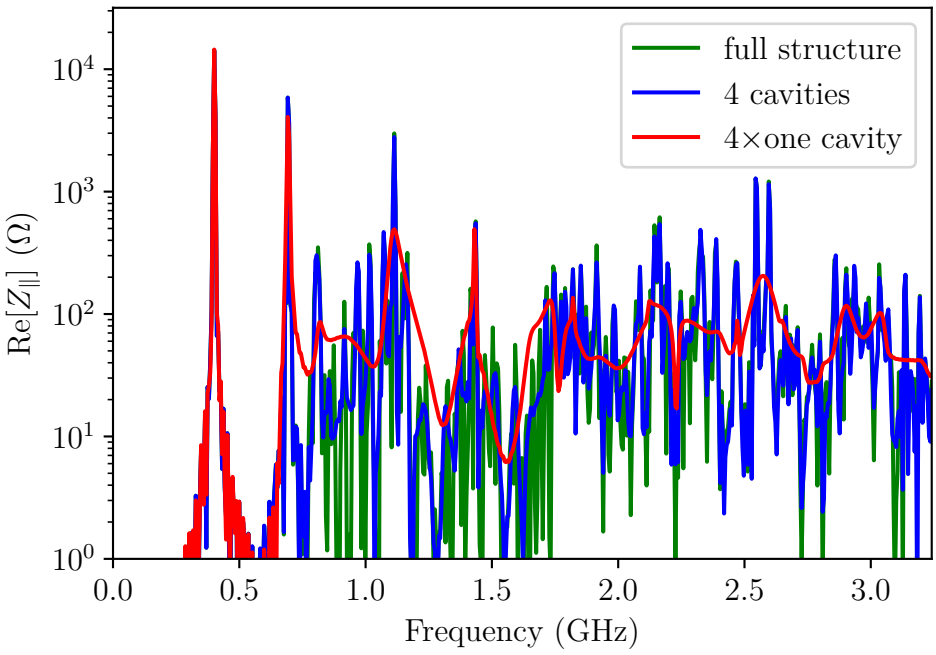

Fig. 12: Comparison of impedance spectra of the full structure containing four single-cell cavities with tapers, four cavities without tapers, and the impedance spectrum of the single-cell cavity multiplied by a factor of 4.

Table 4: The loss factor of different structures obtained with ABCI code. The loss factor of four single-cell cavities is $\kappa_{4\text{cav}} = 1.22$ V/pC. The estimated values are given by Eq. (9), Eq. (8), and Eq. (12).

Loss factor [V/pC]			
Structure	Steps	Taper-out	Tapers
without cavities			
simulations	3.23	1.62	0.28
estimations	2.93	1.47	0.17
with cavities			
simulations	3.82	2.87	1.68
estimations	4.15	2.69	1.39

4 Power loss results

4.1 Power loss from continuous spectrum

4.1.1 Dependence on the number of cells

The power loss calculations for the frequencies above f_{cut} were done for parameters listed in Table 1. The results for the latest parameters with the maximum bunch spacing for each machine and a single train in the ring are summarized in Fig. 13. As expected the Z machine has the highest power loss. The four-cell cavity design is very difficult for this machine because the maximum extracted power of a single coupler is around 1 kW (maximum 6 couplers per cavity). The power deposited in a single-cell cavity can be extracted and this design is used for calculations discussed below. For other FCC-ee machines the power losses are below 1 kW and

only for the W machine in the four-cell cavity $P \approx 1.5$ kW.

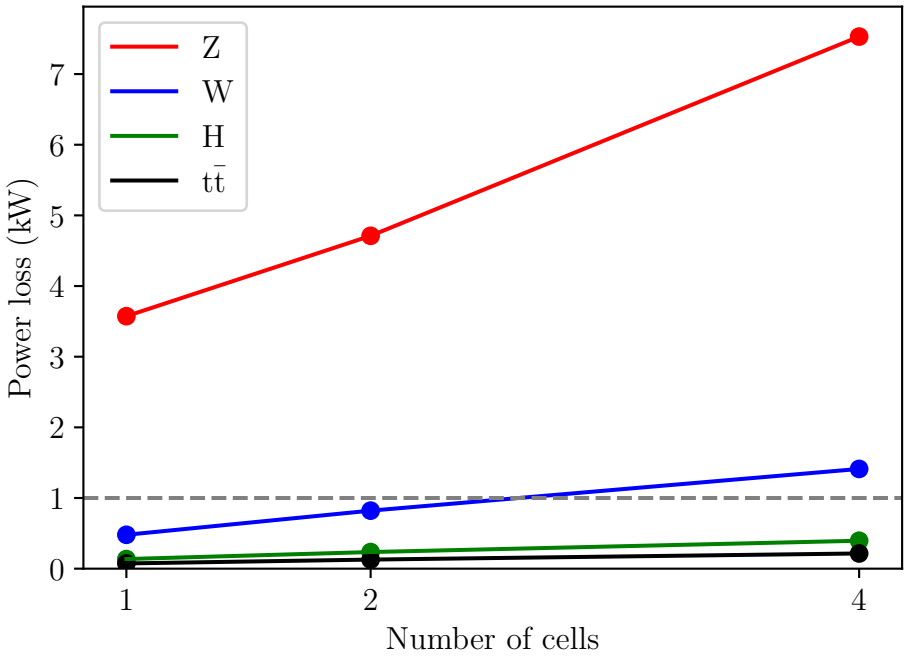

Fig. 13: Power losses for different number of cells in FCC-ee machines (the latest parameters in Table 1). The horizontal line is the maximum power which can be extracted by a single HOM coupler.

Below we analyze the role of different filling schemes for the earlier set of parameters of the Z machine because of a large total number of bunches. The following parameters are assumed to be constant in calculations:

- the total beam current,
- the abort gap length (2 μs),
- the bunch population,
- the bunch length,
- the bunch spacing.

Then depending on the train spacing a beam contains different numbers of trains and different numbers of bunches per train. The power loss as a function of $t_{\rm tt}$ is shown in the left-hand side plot in Fig. 14. The power losses deviate from the value calculated for a single train (the red line) for small distance between trains and then saturate to this value for larger train spacings. The deviations are mostly due to variation of the beam current (see the right-hand side plot in Fig. 14).

For the latest parameters we see that the power loss weakly depends on the bunch spacing (Fig. 15). Slightly higher values for higher $t_{\rm bb}$ are due to hitting of some resonances above cutoff frequency by one of the spectral lines $1/t_{\rm bb}$. The power losses for colliding beams are still possible to extract while for non-colliding beams ($\sigma = 12$ ps) the power absorption could be difficult.

4.1.2 Contribution of tapers

The taper loss factor and the optimum length depend on the ratio d/b of larger and smaller pipe radii. For the transition from $d = 15$ cm to $b = 5$ cm the required taper length is about 3 m

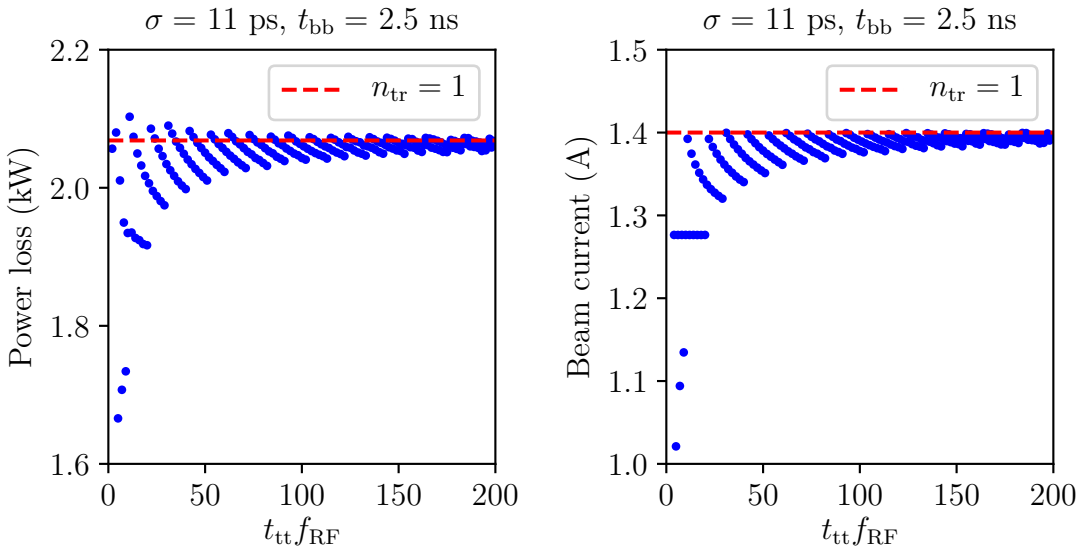

Fig. 14: Dependence of the power loss from continuous impedance spectrum (the left-hand side plot) and the total beam current (the right-hand side plot) on the bunch train spacing. The horizontal dashed lines are the values for a single train. Calculations are done for the earlier set of parameters of the Z machine.

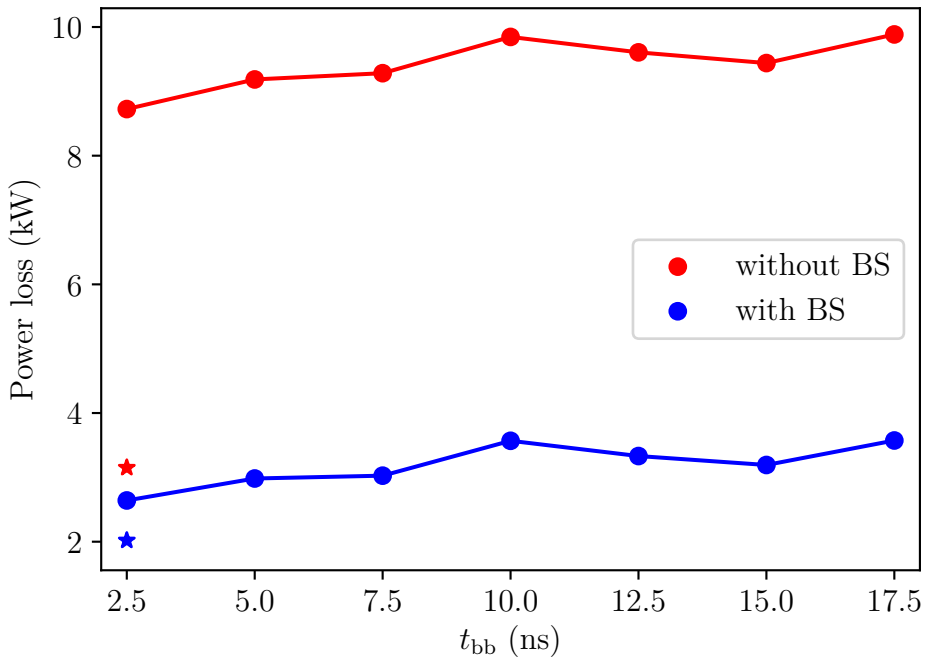

Fig. 15: Power losses for the latest parameters of the Z machine (colliding and non-colliding beams) as a function of the bunch spacing. The stars indicate the values for the earlier set of parameters.

which is not feasible because the taper length would be as long as the length of four cavities in the cryomodule. It means that the taper geometry should optimized using analytic predictions from Eq. (8) and Eq. (10). One of the proposals would be to make transitions to an intermediate beam pipe radius $b_{\rm int}$ between cryomodules (containing 4 cavities) in order to keep the ratio d/b small. For example, the required taper length is about 0.8 m for $b_{\rm int} = 10$ cm which can fit in the cryomodule (Fig. 16). Then additional tapers from the intermediate radius to beam pipe

with radius of 5 cm can used only in places where it is necessary (for example, at the end of straight section for the RF system). The intermediate beam pipe radius should be chosen taking into account the aperture size in the quadrupole magnets, vacuum limitations, and the quality factor of the fundamental mode.

According to Eqs. (9, 10), the loss factor and the optimum taper length are inversely proportional to the bunch length. As bunches of colliding beams for the latest parameter set are almost three times longer than for the earlier one, shorter tapers can be used (see Fig. 16).

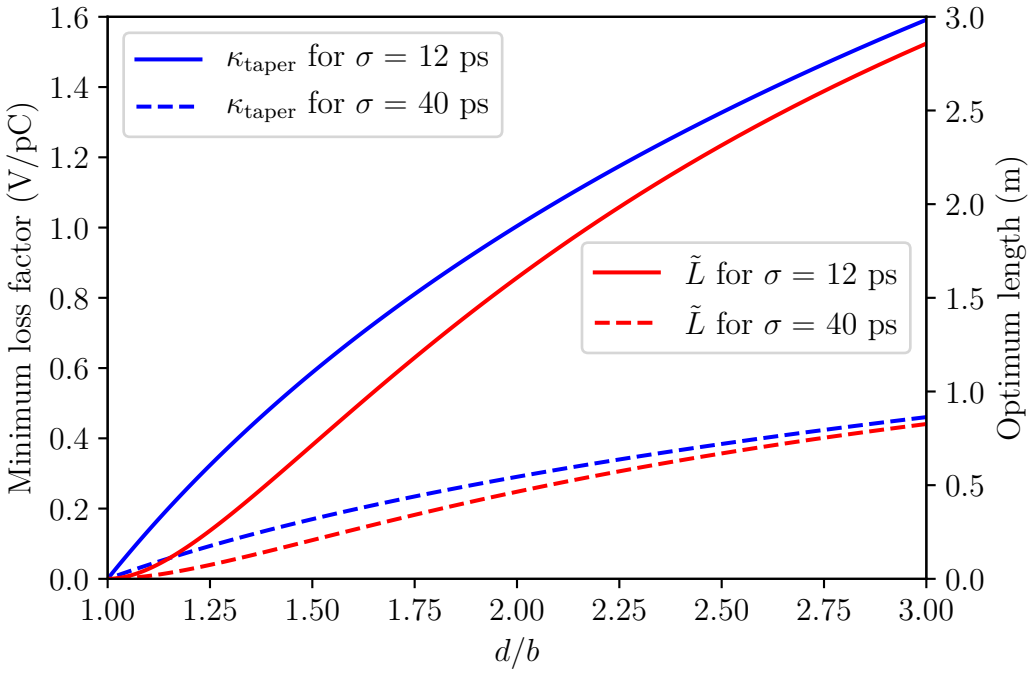

Fig. 16: The minimum loss factor of a taper-out and the optimum taper length as a function of d/b obtained from Eqs. (Eq. (8), Eq. (10)) for the earliest and the latest parameter sets of the Z machine.

4.2 Power loss from discrete cavity spectrum

4.2.1 Hitting of cavity resonances by $1/t_{\rm bb}$ beam spectral harmonics

According to simulation results obtained with ABCI and CST EMS several HOMs are below the cutoff frequency (see in Subsec. 3.1). These modes have large R/Q and Q values and can significantly contribute to the power loss in the case of hitting the high-amplitude beam spectral line.

We consider the worst-case scenario when the HOMs sit at the harmonic of the bunch spacing spectral line $1/t_{\rm bb}$. We assume first that all HOMs are damped to $Q = 10^4$ and evaluate the power loss for all FCC-ee machines (the latest parameters) using HOM parameters listed in Table 3. The results of calculations are summarized in Table 5. The highest power losses for all modes are for the Z machine ($P > 100$ kW) which means that cases of hitting the bunch spacing spectral lines should be avoided. For the W machine the power loss P can be up to 15 kW, while for $Q = 10^3$ the maximum power loss can be kept below 1.5 kW. As the high-energy machines (H and $\rm t\bar{t}$) have a small beam current, the power loss is significantly lower and can be easily extracted by HOM couplers.

In cases of high shunt impedance, reduction of the HOM quality factor is necessary to maintain longitudinal beam stability, which requires the instability growth time $\tau_{\rm inst}$ to be longer

Table 5: The worst-case scenario (HOM coincides with the bunch spacing frequency) for the power loss due to HOMs. Calculations are done for the HOM parameters given in Table 3 assuming of $Q = 10^4$.

	Power loss [W]			
HOM	Z	W	H	$t\bar{t}$
single-cell cavity				
1	4.5×10^5	5.1×10^3	200	10
two-cell cavity				
1	1.9×10^5	2.1×10^3	83	4
2	8.7×10^5	9.8×10^3	380	18
four-cell cavity				
1	6.7×10^3	75	3	0.1
2	9.9×10^4	1.1×10^3	43	2
3	9.5×10^5	1.1×10^4	410	20
4	1.3×10^6	1.5×10^4	580	28

than the synchrotron radiation damping time $\tau_{\rm SR}$. For the case of longitudinal coupled bunch instability, one can use the following estimation [10]

$$\tau_{\rm inst} = \frac{2EQ_s}{e|\eta|J_A f_{\rm r}(R/Q)Q} > \tau_{\rm SR}\ , \tag{13}$$

where $\eta = \alpha_p - 1/\gamma^2$ is the slip factor. Eq. (13) gives the maximum value of the shunt impedance at a given resonant frequency $f_{\rm r}$ when the beam is stable. As the growth time is inversely proportional to the beam current it is shortest for the Z machine. For this machine we consider a single-cell cavity design with the accelerator gradient around 2 MV/cavity. To get the total accelerating voltage of 100 MV (255 MV for the earlier set of parameters) the total number of cavities should be 52 (132 for the earlier set of parameters) because they are combined by four in cryomodules. This gives the limit for the shunt impedance as a function of frequency $5.2\ \mathrm{k\Omega}/f_{\rm r}$[GHz] ($3.3\ \mathrm{k\Omega}/f_{\rm r}$[GHz] for the earlier set of parameters). For the latest and the earlier sets of parameters the HOM of the single-cell cavity should be damped to $Q = 640$ and $Q = 410$, correspondingly. In this case, the power loss still can not be extracted if the bunch spacing spectral line hits the HOM.

4.2.2 Power loss for different filling schemes

As was already discussed in Sec. 2, in the presence of trains the beam spectrum also contains $1/t_{\rm tt}$ spectral lines. Some of these lines can hit the cavity resonances and lead to significant power losses. Here we discuss how to identify such situations, and finally draw conclusions for the cavity design and machine filling schemes.

We focus only on the power loss in the Z machine for the single-cell cavity design. For the earlier set of parameters the power loss map was calculated varying on the distance between trains $t_{\rm tt}$ and the quality factor of the HOM (mode 1 in Table 3). For small Q, power losses are around a few hundred watts and do not depend on $t_{\rm tt}$ (Fig. 17). In this case the impedance is broadband and overlaps with beam spectral lines. There are also several values of $t_{\rm tt}$ with large power losses for high Q. This corresponds to the situation when one of the additional spectral

lines hits the resonance impedance. In the intermediate region moderate losses around a few tens of watts are observed.

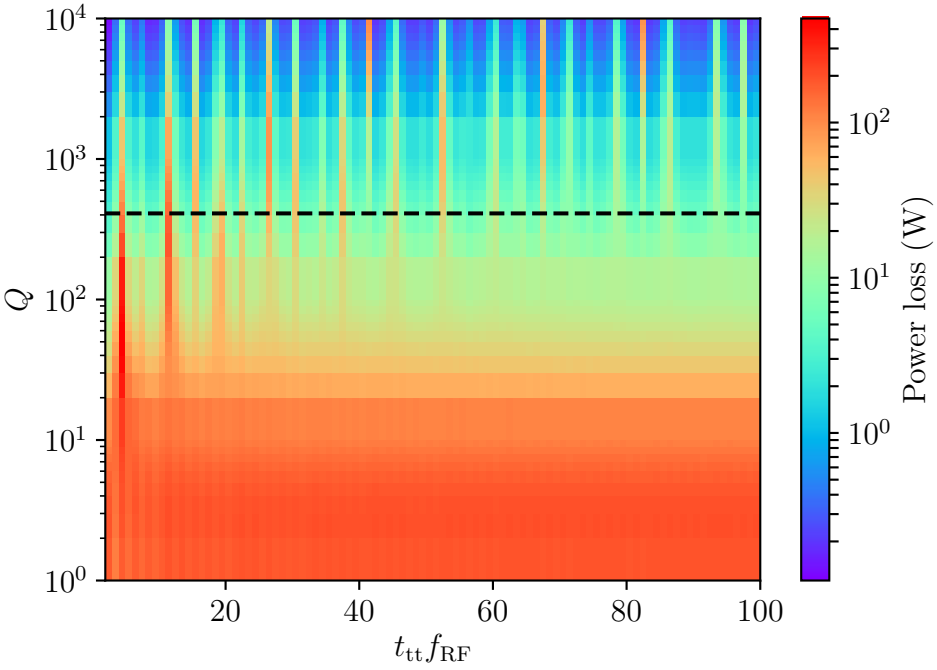

Fig. 17: Power losses from the HOM in the single-cell cavity (mode 1 in Table 3) for different train spacings $t_{\rm tt}$ and different quality factors Q. Calculations are done for the earlier set of parameters of the Z machine. The dashed black line indicates the quality factor required for the longitudinal stability.

To identify the cases when the additional spectral lines hit the resonant line (below referred to as "resonant" cases), the following equation was used

$$\left| 1 - \frac{[f_{\rm r} t_{\rm tt}]}{f_{\rm r} t_{\rm tt}} \right| < \frac{1}{Q} \,, \tag{14}$$

where $[f_{\rm r} t_{\rm tt}]$ denote the rounded off value. Due to manufacturing uncertainties each cavity will have slightly different frequencies of HOMs. This need to be taken into account for the power loss calculation. For each train spacing we vary the frequency of the considered mode with a maximum shift $\Delta f_{\rm r}$ and identify resonant cases using Eq. (14). We see that many resonant cases are present (Fig. 18), but one should not expect a high power loss for all train spacings. To demonstrate this we make a scan of the resonant frequency $f_{\rm r} = 694 \pm 5$ MHz of the damped mode ($R/Q = 12\ \Omega$ and $Q = 410$) with a step of 1 kHz for different filling schemes. For each train spacing we choose the highest power loss and show the results in Fig. 19. The calculated power is below 1 kW for all $t_{\rm tt}$ and for larger train spacing it becomes smaller because the amplitude of additional spectral lines decreases for smaller number of trains $n_{\rm tr}$, see Eq. (4). It means that this mode is not dangerous for the earlier set of parameters of the Z machine .

For the latest parameters the results of calculations for different bunch spacings as a function of the train spacing are shown in Fig. 20. The power losses are always above 1 kW for $t_{\rm bb} = 10$ ns and $t_{\rm bb} = 17.5$ ns because one of the $1/t_{\rm bb}$ spectral lines is close to the HOM. It means that for the present single-cell cavity design these bunch spacings should also be avoided in operation. For other bunch spacings power losses are above 1 kW for $t_{\rm tt} f_{\rm RF} < 75$ which means these filling schemes should be avoided in machine operation. For larger train spacings power losses are below 1 kW.

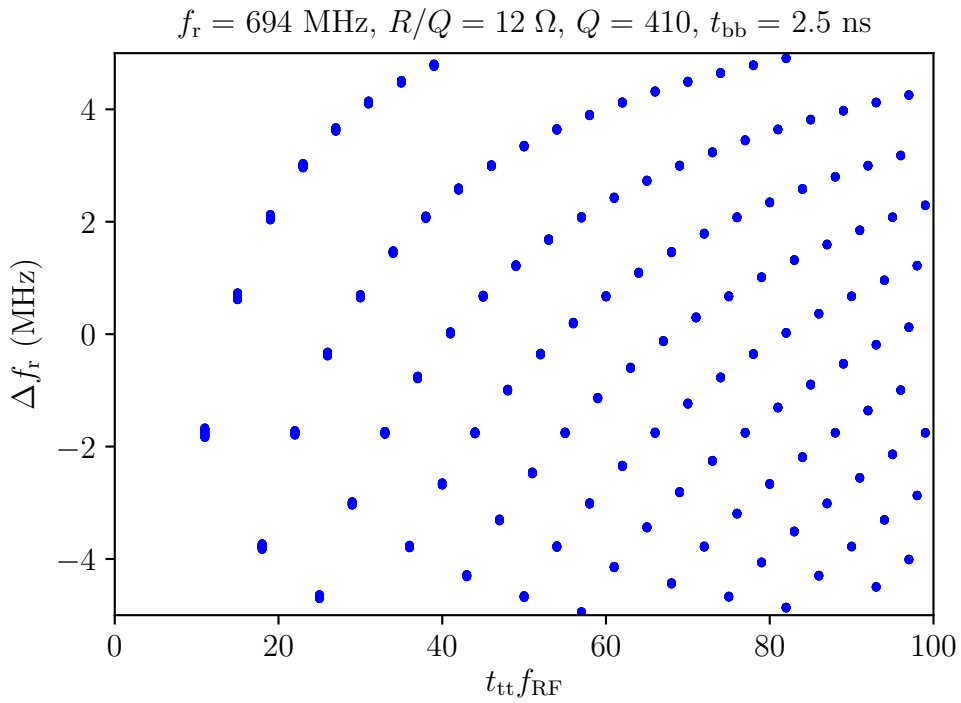

Fig. 18: Cases when the spectral line hits the HOM with frequency variation ± 5 MHz. Calculations are done for the earlier set of parameters of the Z machine using Eq. (14) .

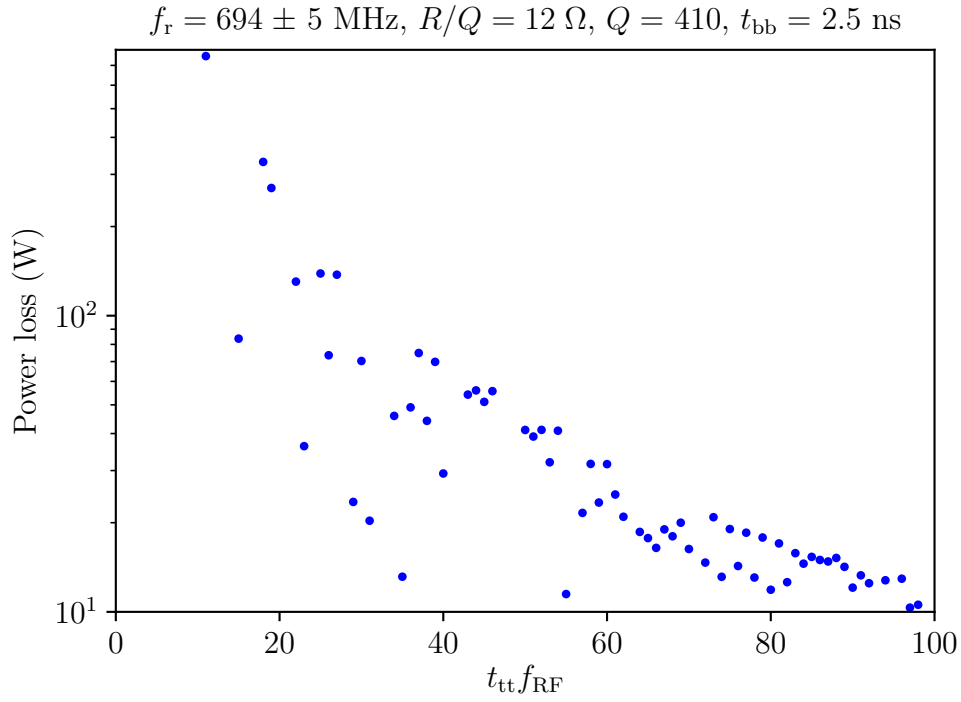

Fig. 19: Dependence of the maximum power loss in resonant cases for the single-cell cavity HOM on the train spacing. The results are obtained from the scan of resonant frequency with the maximum frequency shift of 5 MHz and the frequency step of 3 kHz (the earlier set of parameters of the Z machine).

If the HOM frequency is far enough from one of the $1/t_{bb}$ spectral lines significant power losses can be avoided. This defines a "safe" frequency range with a small power loss for a given bunch spacing. To identify this region we place the resonance frequency between two bunch

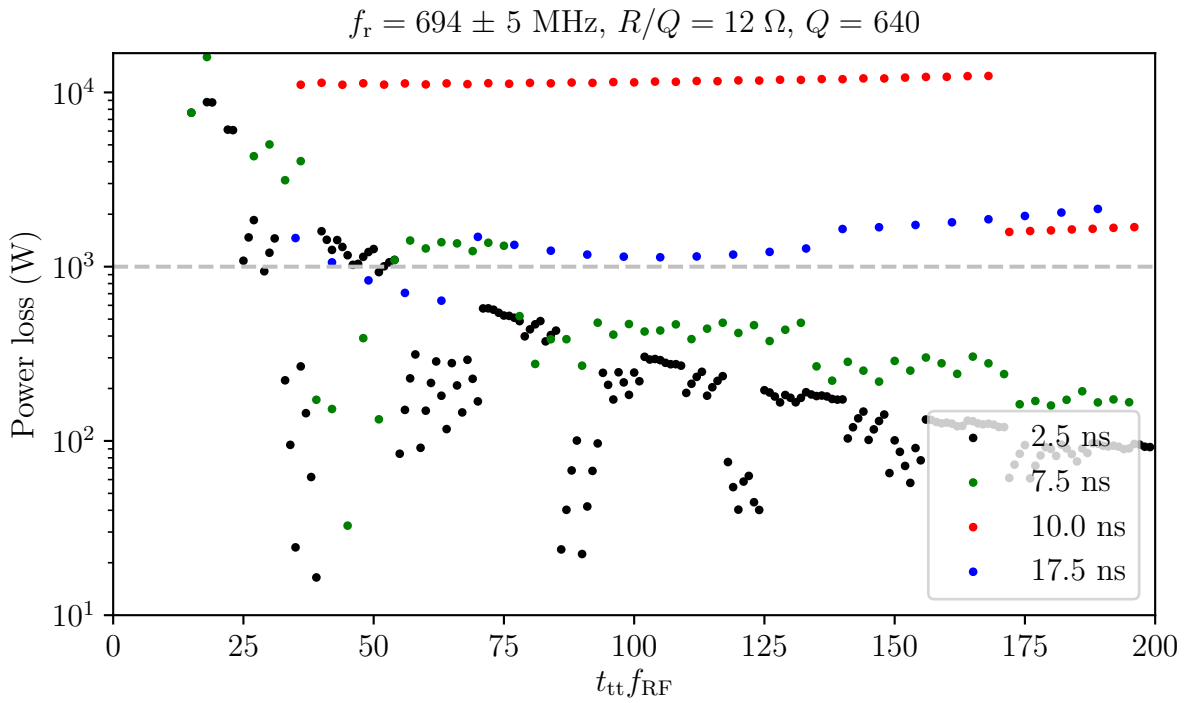

Fig. 20: Dependence of the maximum power loss in resonant cases on the train spacing for the latest parameters of the Z machine and different bunch spacings. The horizontal line shows the limit of 1 kW. For bunch spacings $t_{bb} = 5$, 12.5, 15 ns the behavior of the power losses is similar to $t_{bb} = 2.5$ ns (the black dots) and the power losses are below the values corresponding to $t_{bb} = 7.5$ ns.

spacing spectral lines, vary the frequency shift Δf_r, and calculate the power loss as a function of the train spacing. For larger frequency shifts the larger train spacings are required to keep power losses below 1 kW according to calculations with the latest parameters and $t_{bb} = 2.5$ ns (Fig. 21). It means that if the power loss limit is fixed, the number of train spacings which should be avoided in operation depends on Δf_r. Thus, a certain criteria to fix either Δf_r or t_{tt} should be used. From the total beam current we see that for short distances between trains it can be too low for all bunch spacings (see Fig. 22). The 5% deviation of the beam current from the nominal leads to the condition $t_{tt} f_{RF} > 100$. Assuming that short train spacings ($t_{tt} f_{RF} < 100$) should be avoided in operation, frequency ranges with acceptable power losses for all bunch spacings can be defined. The results are shown in Fig. 23. These regions are different for different t_{bb}. One can see also that it is difficult to find the frequency of HOM which is suitable for all bunch spacing (see, for example, the position of HOM for the present single-cell cavity design). By excluding one of the bunch spacings these regions can be expanded giving more flexibility for possible cavity designs.

5 Conclusions

The beam-induced power loss estimations for accelerating structures are necessary to avoid damage of their components. In this work semi-analytical and simulation tools were used to evaluate the cavity designs for FCC-ee machines with this objective.

Calculations were done using the analytic beam spectrum with regular filling schemes and an impedance spectrum obtained with ABCI code for the 400.79 MHz cavity design similar to LHC. Considering the power loss from the continuous spectrum above cutoff frequency, all cavity designs (single-cell, two-cell, and four-cell) can be used for W, H, $t\bar{t}$ machines since

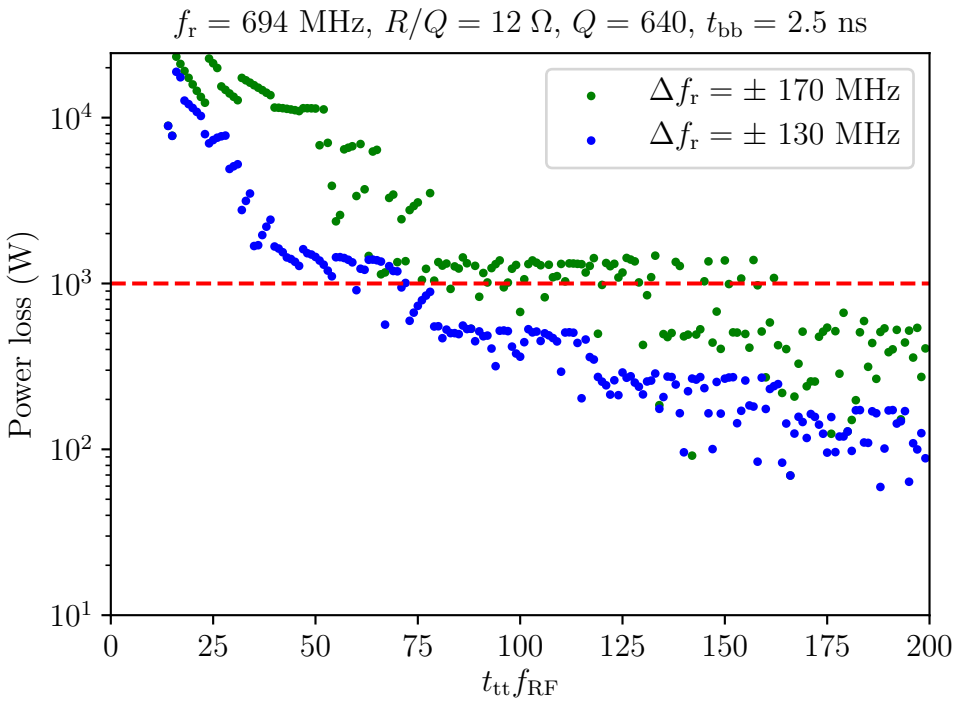

Fig. 21: Dependence of the maximum power loss in the resonant cases on the train spacing for different frequency shift of HOM. For each train spacing the frequency of the mode was varied with the step of 3 kHz. For each train spacing, results are obtained from the scan of the resonant frequency with a step of 10 kHz. The horizontal line is the limit of 1 kW.

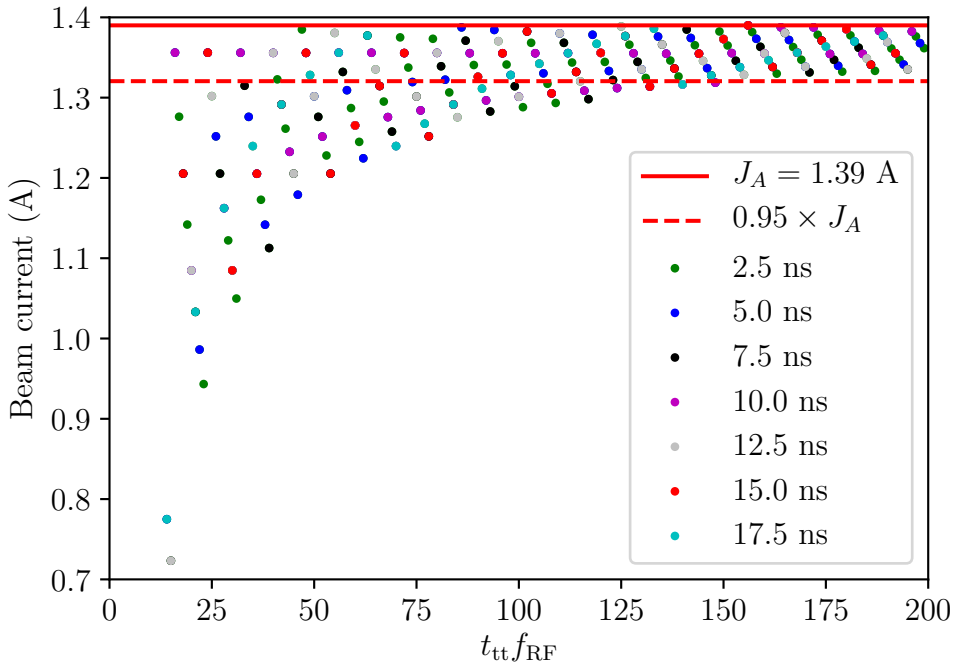

Fig. 22: Dependence of the total beam current in the resonant cases on the train spacing for different bunch spacings.

power losses are below or around 1.5 kW. However only single-cell cavity design is feasible for the Z machine. For the earlier set of parameters the values are around 2 kW and 3 kW for the case of colliding and non-colliding beams respectively which can be extracted by several HOM

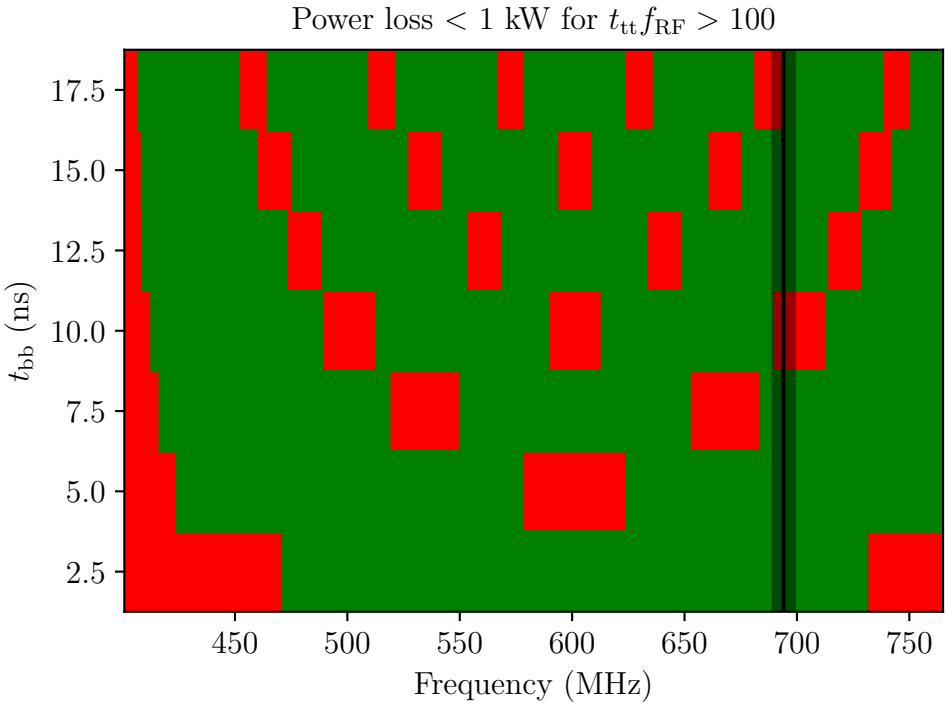

Fig. 23: Frequency ranges with acceptable power losses below 1 kW for different bunch spacings (green regions). Regions with power losses above 1 kW are shown with red color. The vertical line corresponds to the position of HOM of the single-cell cavity design with the maximum frequency shift of 5 MHz. The considered frequency range is limited by the frequency (400.79 MHz) of the fundamental mode and the cutoff frequency (765 MHz).

couplers (the maximum power 1 kW/coupler). For the latest parameters, power losses slightly depend on the bunch spacing due to hitting of some resonances above cutoff frequency by one of the bunch spacing spectral lines. Calculations for non-colliding, shorter beams show high power losses (around 9 kW), which could be difficult to extract.

Tapers can significantly contribute to the high-frequency part of the impedance spectrum. This results in an increase of the power loss which can be reduced by using tapers with proper dimensions which depends on the bunch length. For the earlier set of parameters of the Z machine, the transitions between 15 cm and 5 cm pipe radii should be done using 3 m long tapers, which is unphysical. A distance between taper-out and taper-in should be at least 6 m to achieve cancellation of their contributions to the total power loss. Making transitions from 15 cm beam pipe to the intermediate radius of 10 cm where possible would allow us to use tapers with the length below 1 m and place them in the cryomodules. The taper dimensions can be reduced for the latest parameters with longer bunches.

The HOMs with a large ratio of the shunt impedance to the quality factor R/Q are present in the cavity impedance for frequencies below the cutoff frequency, according to ABCI and CST EMS simulations. The hitting of one of the HOMs by a bunch spacing spectral line can result in a large power loss. For the latest FCC-ee machine parameters this worst-case scenario was evaluated assuming of the quality factor $Q = 10^4$ for all modes. The power losses for high energy machines are small because of a low beam current. For the W machine and the four-cell cavity design (with the highest impedance) it can be kept below 1.5 kW by further reduction of the quality factor to 10^3. The most challenging is the Z machine, where power losses could be above 100 kW. For the latest parameters and the damped HOM ($Q = 640$ is required for longitudinal beam stability) power loss is about 30 kW. To avoid large power losses in this machine, the cavity should be designed in a way that the bunch spacing spectral lines do not hit

HOMs.

Different filling patterns modify the beam spectrum. We identified the cases when additional spectral lines due to the train spacing can hit the impedance resonances. For the earlier set of machine parameters and the single-cell cavity design with the damped HOM (the resonant frequency around 694 MHz and the maximum frequency shift ± 5 MHz), power losses are not dangerous for any train spacings. For the latest parameters, 10 ns and 17.5 ns bunch spacings are not feasible for the considered HOM. For other bunch spacings, the train spacings smaller than 75 RF buckets should be avoided in operation.

Finally, the frequency range for the considered HOM of the single-cell cavity design was calculated where power losses are below 1 kW for the train spacings longer than 100 RF buckets. The width of these frequency ranges depends on the bunch spacing. The overlap of safe regions is possible by excluding some of the bunch spacings in operation. This strategy can be used as recommendations for new cavity designs with range for HOM frequencies defined by requirements from machine operation.

Acknowledgements

We would like to thank Andrew Butterworth, Olivier Brunner and Nikolay Schwerg for useful discussions and collaborations. The special acknowledgments go to Juan Esteban Müller who previously worked on this topic. We also thank Dmitry Teytelman and Robert Rimmer for the comments about filling schemes.

References

[1] F. Zimmermann, D. Shatilov, K. Oide, and K. Ohmi, "FCC-ee Parameter Changes since Berlin Meeting," *49th FCC Coordination Group Meeting*, no. August, 2017.

[2] J. Wenninger, M. Benedikt, K. Oide, and F. Zimmermann, "Future Circular Collider Study Lepton Collider Parameters," *Report FCC-ACC-SPC-000X*, 2017.

[3] F. Caspers, C. Gonzalez, M. D'yachkov, E. Shaposhnikova, and H. Tsutsui, "Impedance Measurement of the SPS MKE Kicker by means of the Coaxial Wire Method," *Cern Report PS/RF/Note 2000-004*, 2000.

[4] D. Boussard and T. Linnecar, "The LHC superconducting RF system," *Cryog. Eng. Int. Cryog. Mater. Conf. (CEC-ICMC'99), 12-16 July 1999, Montr. Canada*, no. July 1999, pp. 12–16.

[5] Yong Ho Chin, "ABCI (Azimuthal Beam Cavity Interaction) code."

[6] "CST EM STUDIO, https://www.cst.com/products/cstems."

[7] A. M. Al-Khateeb, "Longitudinal geometric loss factor and impedance of a step-out discontinuity at arbitrary beam energy in a round cylindrical beam-pipe," *Nucl. Instruments Methods Phys. Res. Sect. A Accel. Spectrometers, Detect. Assoc. Equip.*, vol. 635, pp. 35–40, apr 2011.

[8] S. A. Heifets and S. A. Kheifets, "Coupling impedance in modern accelerators," *Rev. Mod. Phys.*, vol. 63, pp. 631–673, jul 1991.

[9] A. Blednykh and S. Krinsky, "Loss factor for short bunches in azimuthally symmetric tapered structures," *Phys. Rev. ST Accel. Beams*, vol. 13, no. 6, pp. 1–6, 2010.

[10] K. Y. Ng, *Longitudinal Coupled-Bunch Instabilities*, pp. 311–314. World Scientific Publishing Co. Re. Ltd., 2006.